



Differentiation of ferrocene D_{5d} and D_{5h} conformers using IR spectroscopy

Narges Mohammadi^a, Aravindhnan Ganesan^a, Christopher T. Chantler^b, Feng Wang^{a,*}

^a eChemistry Laboratory, Faculty of Life and Social Sciences, Swinburne University of Technology, Hawthorn, Melbourne, Victoria 3122, Australia

^b School of Physics, University of Melbourne, Parkville, Victoria 3052, Australia

ARTICLE INFO

Article history:

Received 27 January 2012

Received in revised form

21 March 2012

Accepted 10 April 2012

Keywords:

Ferrocene conformers

Eclipsed and staggered

DFT calculations

IR spectral fingerprint

Molecular electrostatic potentials (MEP)

Iron involved properties

ABSTRACT

Fingerprinting in the infrared (IR) spectral region of 450–500 cm^{-1} of ferrocene is discovered to be a sensitive way to differentiate the eclipsed (D_{5h}) and staggered (D_{5d}) conformers of ferrocene. The present study simulates accurate IR spectra for ferrocene using density functional theory (DFT) based on the B3LYP/m6-31G(d) model without any scaling and manipulation. The agreement with an early experiment and other theory is excellent. It is found that in the vacuum, the eclipsed conformer represents the true minimum structure of ferrocene, whereas the staggered conformer represents the saddle point structure, in agreement with a number of other theoretical and experimental studies. The study further reveals that the sandwich complexes are formed by stacking two Cp rings with an Fe atom in the middle and there are no conventionally localised Fe–C bonds in ferrocene. The vibrational frequency splitting of $\Delta\nu = 17 \text{ cm}^{-1}$ in the IR region of 450–500 cm^{-1} (expt. $\Delta\nu = 16 \text{ cm}^{-1}$) becomes the fingerprint of the eclipsed conformer in contrast with the staggered conformer of ferrocene. In addition, the present study suggests that the earlier IR spectral measurement of Lippincott and Nelson (1958) of ferrocene was not D_{5d} alone but was likely a mixture of both eclipsed and staggered ferrocene. Finally, the study highlights that Fe-related properties of ferrocene hold the key to reveal one ferrocene conformer from the other.

© 2012 Elsevier B.V. All rights reserved.

1. Introduction

The discovery of ferrocene $\text{Fe}(\text{C}_5\text{H}_5)_2$, i.e., di-cyclopentadienyl iron (FeCp_2 or Fc), is usually regarded as the establishment of contemporary organometallic chemistry, which is probably the reason why the sandwich structure is indicated by the cover of the Journal of Organometallic Chemistry. Since its discovery some fifty years ago [1], a literature search in 2010 yields over 23,000 articles studying ferrocene [2] and new discoveries of ferrocene continue. For example, a most recent article in Nature Chemistry established ferrocene as a redox couple for organic dye sensitizer solar cell (DSSC) [3]. The preparation of ferrocene has stimulated an immense amount of studies on cyclopentadienyl (Cp) and other symmetrically delocalized hydrocarbon metal complexes with a unique sandwich molecular structure, strong metal-ring π bonding, facile redox behaviour, and ease of derivatization [4]. Ferrocene derivatives have been synthesized with wide application in areas such as homogeneous catalysis, polymer chemistry, molecular sensing, and nonlinear optical materials [5]. In biology, ferrocenium species are among many organometallic compounds

found to have antineoplastic activity [6]. This activity is thought to arise from the generation of reactive oxygen species that damage DNA [7].

As a prototypical metallocene with a sandwich structure, ferrocene exhibits only a small energy barrier separating the staggered (D_{5d} symmetry) and eclipsed (D_{5h} symmetry) rotational orientations of the parallel cyclopentadienyl rings [8]. The development of ferrocene study since its discovery in 1951 [1] has been well documented in recent articles such as Coriani et al. [9], Roy et al. [10], Gryaznova et al. [11] and Bean et al. [2]. It has been stated [11] that a staggered ferrocene structure of D_{5d} point group symmetry dominates experiments in the condensed phase [12–15], whereas the eclipsed structure of D_{5h} point group symmetry is found in the gas phase [16–18]. The eclipsed conformation was also observed at 90 K in the solid [19] and at room temperature in solutions [20]. As most of the theoretical studies of ferrocene refer to gas phase or solutions, the eclipsed (D_{5h}) structure of ferrocene has been more extensively studied than the D_{5d} conformer.

Study of ferrocene conformers will help our understanding of other metallocenes and their derivatives with applications in biotechnology, nanotechnology and solar technology [20]. For example, Cooper et al. [21] recently developed a class of ferrocene synthons which may add to the number for organometallics with

* Corresponding author. Tel.: +61 3 9214 5065; fax: +61 3 9214 5921.

E-mail address: fwang@swin.edu.au (F. Wang).

useful medicinal properties [22]. The rotational energy barriers with respect to the metal–cyclopentadienyl axis between the eclipsed and staggered conformers are very low [20,23], as a result, it is possible that the ground electron state structures of ferrocene may contain both of the conformations. The fact that electronic structures and properties of the ferrocene conformers are strikingly similar is a key hurdle to differentiate or separate the configurations from one another. However, detailed studies of D_{5h} and D_{5d} of ferrocene are important as ferrocene derivatives may inherit particular properties which only exist in one conformer [23]. For example, additional ligands coordinating to the metal and the Cp rings while maintaining certain symmetry, can be a geometric requirement for the D_{5h} conformer [21]. In addition, the understanding of synthesis pathways, mechanics and reaction dynamics of the ferrocene derivatives will require the understanding of the structure, symmetry and properties of the ferrocene conformers.

Density functional theory has been revealed as cost effective and accurate method to study electronic structures and properties of ferrocene [9,11]. It begins to recognize that the CpFeCp structure does not confine to the conventional Fe–C “bonds” [2]. Infrared (IR) spectra of ferrocene [11,24] reveal torsional or swing vibrations of CpFeCp in the low energy region of $<600\text{ cm}^{-1}$, indicating that it is unlikely that such ten localised Fe–C bonds exist in the ferrocene structures as proposed [9–11,24]. Rather, the most likely structures for both D_{5h} and D_{5d} conformers of ferrocene can be structures of stacking two pentagon Cp rings in two orientations. The stacking structures are able to explain why the IR spectra could observe CpFeCp swing vibrations in low energy IR regions [24]. Furthermore, Gryaznova et al. [11] revealed that the DFT simulated IR spectra of ferrocene are reliable and can be employed to diagnose

the spin state ($S = 0$) of the transition metal (Fe) complexes. The IR spectra of CpFeCp have been measured in both vapour and solution with reasonably good resolution in the region of $400\text{--}4000\text{ cm}^{-1}$ over half a century ago [24]. As limited by accurate theoretical support at the time of this early experiment, their analyses assumed that the observed IR spectra belong to the D_{5d} conformer of ferrocene [24]. In fact the actual measured IR spectra indicated the opposite, that is, the D_{5h} (eclipsed) ferrocene conformer domination in vapour state due to the observed spectral peak splitting in the $450\text{--}500\text{ cm}^{-1}$ region. The eclipsed structure for ferrocene is in agreement with a microwave experiment [16] several years later. In the present study, we use simulated IR spectra and a number of other properties of D_{5h} and D_{5d} conformers of ferrocene, combined with available experiments [16–18,24] and other theoretical calculations [9–11] to confirm that the eclipsed conformer dominates the ferrocene in the vapour phase.

2. Computational methods

All calculations are performed using the Gaussian 09 computational chemistry package [25]. Geometry optimizations of the ferrocene conformers are carried out using the B3LYP/m6-31G(d) model. The basis set m6-31G(d), a modified version of the 6-31G(d) [26], is employed in the calculations. This basis set incorporates necessary diffuse d-type functions for the first-row transition metals such as Fe. It exhibits a better performance than the conventional 6-31G(d) basis set for the iron atom in ferrocene by providing a more appropriate description for the important energy difference between the atomic $3d^n4s^1$ and $3d^{n-1}4s^2$ states [27]. The infrared (IR) spectra of the ferrocene conformers are simulated on the optimized structure using the same model.

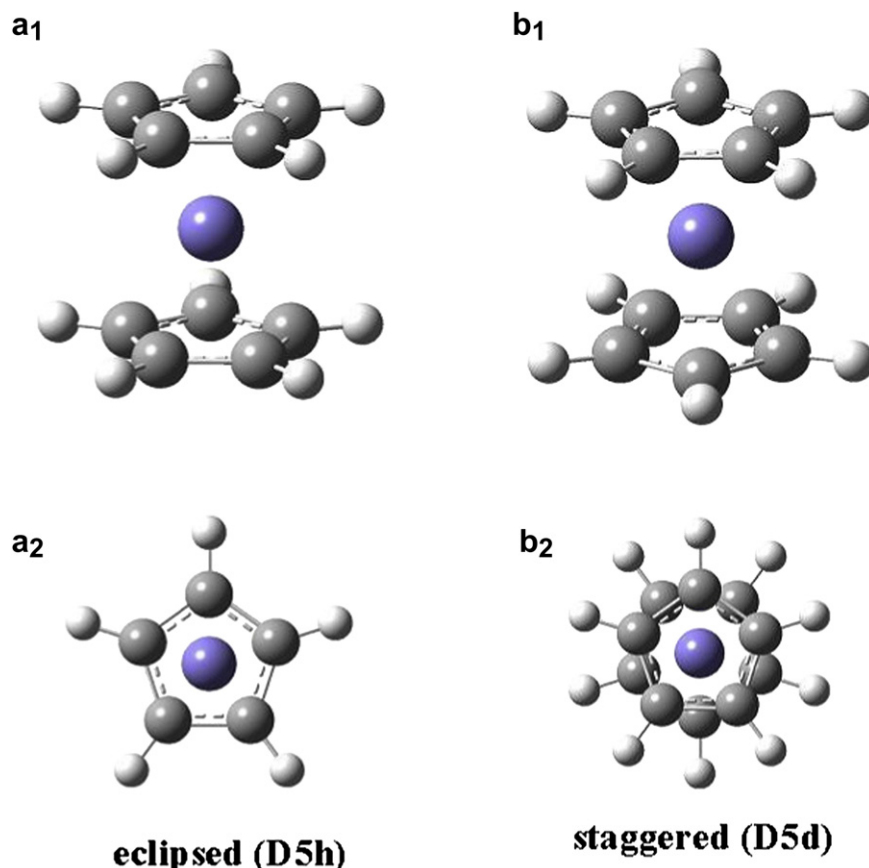


Fig. 1. Optimized molecular structures of the D_{5h} (eclipsed) and D_{5d} (staggered) conformers of ferrocene in three-dimensional (3D) space.

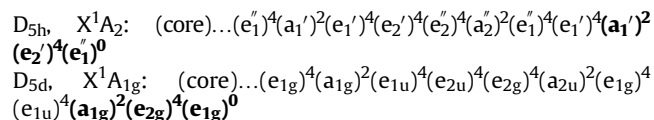
A potential energy scan (PES) is performed by rotating the central cyclopentadienyl axis which is defined by a dihedral angle δ ($C_{(1)}-X_{(2)}-Fe_{(3)}-C_{(4)}$) which connects the centres of each cyclopentadienyl planes through the middle Fe atom. The PES produced from the calculations starts from an eclipsed conformer ($\delta = 0^\circ$) at a step size of $\Delta\delta = 4^\circ$. Due to the pentagonal structure of the Cp ring, every 36° that the dihedral angle rotates will result in an alternative staggered–eclipsed conformation periodically.

3. Results and discussion

3.1. Geometries and PES scan

The optimised geometries of the eclipsed and staggered conformers of ferrocene are given in Fig. 1 as three-dimensional (3D) structures. Our calculations indicate that the eclipsed conformer is a true global minimum structure of ferrocene without imaginary frequencies in isolation, whereas the staggered conformer is the saddle point in the gas phase due to imaginary frequencies. This is in good agreement with other theoretical studies [9–11]. Although the graphic user interface (GUI) tools for computational chemistry packages such as ADFView [28] and Molden [29] almost always indicate the ten localised Fe–C bonds existing in both D_{5h} and D_{5d} conformers of ferrocene in display, the ferrocene orientations are likely to adopt stacking structures due to the ligand π -orbitals and aromaticity as noted by Bean et al. [2]. Infrared (IR) discussion herein will also provide evidences of the stacking structures rather than the conventional Fe–C bonds for ferrocene.

Table 1 compares selected characteristic geometric and electronic properties of D_{5h} and D_{5d} conformers of ferrocene with other theoretical and experimental results. The ground electronic state of ferrocene is a low-spin state as indicated by Gryaznova et al. [11], our B3LYP/m6-31G(d) model gives the configurations as



The major difference between the conformers is due to a symmetric plane for D_{5h} but a symmetric centre for D_{5d} in their point group character tables. As a result, the orbital irreducible representations which are correlated as ' and '' in D_{5h} become g and u in D_{5d} . The highest occupied molecular orbital (HOMO) of D_{5h} conformer is a doubly degenerate e_2' state and the next HOMO (HOMO-1) is a_1' but the lowest unoccupied molecular orbital (LUMO) is e_1' which agrees well with previous DFT based B3LYP/6-31G** calculations [2]. On the other hand, the HOMO for D_{5d} is a doubly degenerate e_{2g} state, the HOMO-1 is a_{1g} and LUMO is e_{1g} . Fig. 2 gives the orbitals of the doubly degenerate HOMOs for D_{5h} (e_2') and for D_{5d} (e_{2g}), as well as the doubly degenerate LUMOs for D_{5h} (e_1') and for D_{5d} (e_{1g}), based on our B3LYP/m6-31G(d) calculations. As can be seen in this figure, although the HOMO–LUMO gaps of the eclipsed and the staggered exhibit a small difference in energy (0.04 eV), the HOMOs and LUMOs of the eclipsed and staggered exhibit major similarities to their corresponding partners, except the bottom Cp of the eclipsed ferrocene orbitals which

Table 1
Comparison of the optimized geometries of eclipsed and staggered ferrocene conformers.

Bond/angle	B3LYP ^a	HF ^b	MP2 ^c	CCSD(T) ^c	B3LYP/Type-1 ^d	Expt. ^e
Eclipsed (D_{5h})						
Fe–C ₅ (Å) ^f	1.670	1.865	1.464	1.655	1.687–1.688	1.660
Fe–C (Å)	2.065	2.219	1.910	2.056	2.079–2.080	2.064 ± 0.003
C–C (Å)	1.428	1.413	1.441	1.433	1.428	1.440 ± 0.002
C–H (Å)	1.082	1.074	1.076	1.077		1.104 ± 0.006
\angle C ₅ –H (Å)	0.66	0.58	0.33	1.03		3.7 ± 0.9 ^g
$E_{\text{total}}(E_h)$	–1650.662 ^h					
$E_{\text{total}} + \text{ZPE}(E_h)$	–1650.492					
$\langle R^2 \rangle$ (a.u.)	1358.84					
μ (Debye)	0.0					
Electronic state	$^1A_1'$					
$\Delta\text{HOMO–LUMO}$ (eV)	5.30					
A,B,C (GHz)	A: 2.19453 B: 1.05862 C: 1.05862					
Staggered (D_{5d})						
Fe–C ₅ (Å)	1.674	1.866	1.487	1.659		
Fe–C (Å)	2.068	2.220	1.925	2.058		
C–C (Å)	1.428	1.413	1.437	1.432		
C–H (Å)	1.082	1.074	1.076	1.077		
\angle C ₅ –H (Å)	0.92	0.55	1.39	1.34		
$E_{\text{total}}(E_h)$	–1650.661 ^h					
$E_{\text{total}} + \text{ZPE}(E_h)$	–1650.491					
$\langle R^2 \rangle$ (a.u.)	1361.78					
μ (Debye)	0.0					
Electronic state	$^1A_{1g}$					
$\Delta\text{HOMO–LUMO}$ (eV)	5.26					
A,B,C (GHz)	A: 2.19455 B: 1.05503 C: 1.05503					

^a This work with the B3LYP/m6-31G(d) model. The basis set is a modified version of 6-31G(d) basis set [26].

^b See [34].

^c See [9].

^d See [11].

^e See [17].

^f Denotes the distance from Fe atom to the centre of cyclopentadienyl ring.

^g See [18]. From an ND experiment (not corrected for thermal motion) the value is 1.7 ± 0.2 [35].

^h Energy difference between D_{5h} and D_{5d} is: $\Delta E = 0.0272 \text{ eV} = 0.62 \text{ kcal mol}^{-1}$ ($0.9 \text{ kcal mol}^{-1}$, expt. [17]).

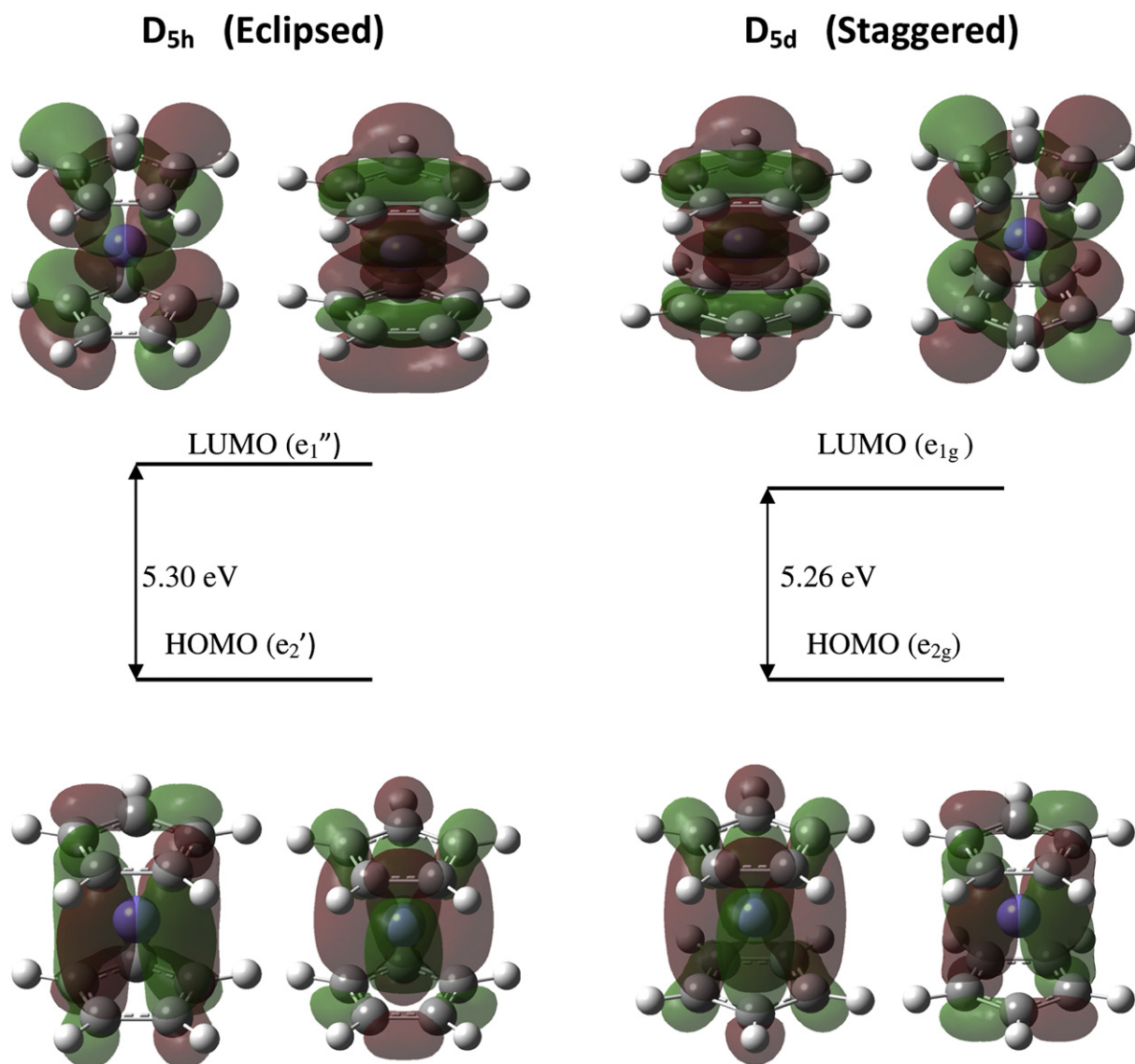


Fig. 2. The highest occupied molecular orbitals (HOMOs) and the lowest unoccupied molecular orbitals (LUMOs) of the eclipsed (D_{5h}) and the staggered (D_{5d}) conformers of ferrocene.

are not mirror reflection of the top part as in the staggered. The HOMOs and LUMOs are dominated by both the iron atom and the carbon atoms of ferrocene. As a result, the differences between the HOMOs and LUMOs are not significant enough to differentiate the conformers.

Fig. 3(a) reports the potential energy scan (PES) of ferrocene when rotating the central cyclopentadienyl axis, i.e., the dihedral angle, δ ($\angle C_{(1)}-X_{(2)}-Fe_{(3)}-C_{(4)}$) where $X_{(2)}$ is a dummy atom located at the centre of the top Cp pentagon plane as shown in Fig. 3(b). As indicated before, due to the pentagonal structure of Cp fragment, rotation of the dihedral angle δ from 0° to 2π will reproduce D_{5h} and D_{5d} five times periodically as the period is $2\pi/5$. The energy difference, ΔE , between D_{5h} and D_{5d} conformers of Fc is given by $0.62 \text{ kcal mol}^{-1}$ using the B3LYP/m6-31G(d) model, comparing to approximately $0.9(3) \text{ kcal mol}^{-1}$ as measured by gas phase electron diffraction (GED) [17]. This result is in agreement with other DFT calculations [9]. Due to their high symmetries, both D_{5h} and D_{5d} conformers do not possess permanent dipole moments. As a result, the IR spectroscopy of ferrocene will be due to induced dipole moments during vibration. The calculated

molecule size (i.e., the electronic spatial extent $\langle R^2 \rangle$ as given in Table 1) of the D_{5d} conformer is slightly larger than the D_{5h} conformer. The former (D_{5d}) is 1361.80 a.u. but the latter (D_{5h}) is 1358.84 a.u. The size of D_{5d} is slightly larger but was found in condensed phase, whereas the smaller size ferrocene D_{5h} is found in gas phase, solid and solution. The energy gap between the HOMO and the LUMO, i.e., $\Delta\epsilon(\text{HOMO-LUMO})$, is given by 5.30 eV and 5.26 eV for D_{5h} and D_{5d} , respectively. However, such small differences in the properties are not sufficient to warrant meaningful investigation for such differences in most measurements. Other properties which can differentiate the conformers sensitively ought to be disclosed.

The optimized geometric parameters for the conformer pairs are almost identical using the same model as shown in Table 1. For example, all C–C bonds are given by 1.428 Å and all C–H bonds are reported as 1.082 Å. The results in Table 1 also indicate that the hydrogen atoms of Cp are not in the same plane with the C_5 pentagon ring. The hydrogen atoms slightly bend towards their counterpart in the opposite Cp ring, again in agreement with experimental findings [18] that the conformer bend angle

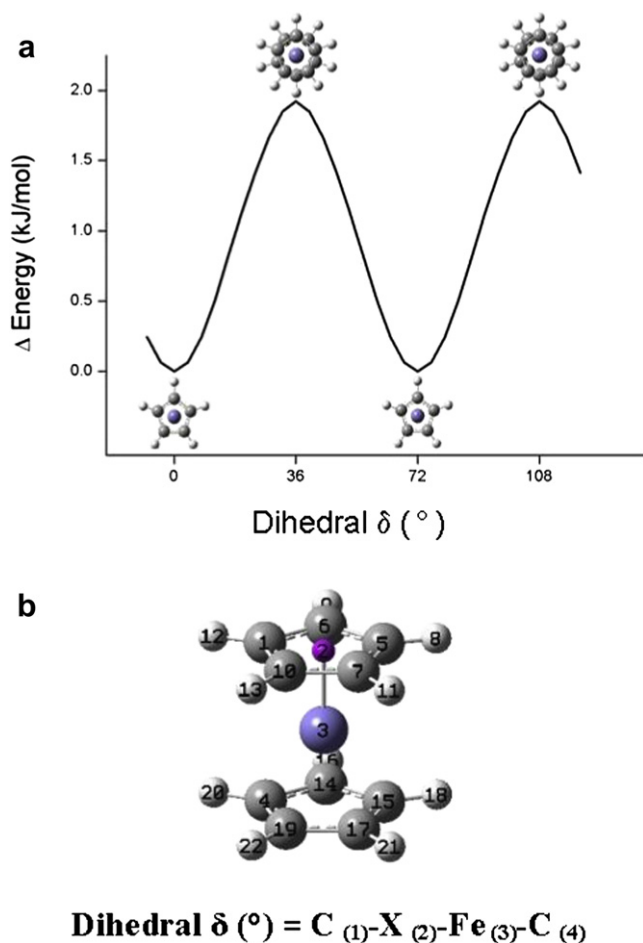


Fig. 3. (a) Potential energy scan (PES) of the dihedral angle rotating the axis connecting the middle Fe atom as well as the centres of two Cp rings. Due to the pentagon structure of Cp, every 36° rotation of the dihedral angle will produce either the D_{5h} or the D_{5d} structure once. This figure only presents a period of the PES. (b) The definition of the dihedral angle.

involving the hydrogen atoms in D_{5h} is $\angle C_5-H = 3.7 \pm 0.9^\circ$. However, calculations indicated that this angle is much smaller than the crystalline structure of D_{5h} of Fc, from $\angle C_5-H = 0.66^\circ$ in B3LYP/m6-31(d) to $\angle C_5-H = 1.03$ in CCSD(T)/TZV2P+f [9]. Theory also indicates that this angle, $\angle C_5-H$, for D_{5d} (0.92° in B3LYP/m6-31(d) and 1.344° in CCSD(T)/6-31G** [9]) is larger than that of D_{5h} . Small differences of the distances between Fe and the Cp rings in D_{5h} and D_{5d} are also observed. The Fe–Cp distance of the latter (D_{5d}) is slightly longer than the Fe–Cp distance in D_{5h} , i.e., 1.674 \AA in D_{5d} whereas in D_{5h} this distance is given by 1.670 \AA .

3.2. Molecular electrostatic potential

Cross-sections of the molecular electrostatic potentials (MEPs) of D_{5h} and D_{5d} conformers are given in Fig. 4. The upper panels, (a₁) and (b₁), are the cross-sections through one of the pentagon Cp rings of the conformers, which are virtually identical in D_{5h} and D_{5d} as only one of the Cp rings is presented in the MEP which is independent of the other Cp ring and their orientation. Perhaps the noticeable difference between (a₁) and (b₁) is that the projection of the opposite Cp ring overlaps with the working Cp ring in D_{5h} , whereas the same projection in the D_{5d} case does not overlap with the working Cp ring due to its reflection centre, *i*.

The middle panels, (a₂) and (b₂) are the MEP cross-sections with an oblique cut through the centre Fe atom. The MEP cross-sections in (a₂) and (b₂) are very different for D_{5h} and D_{5d} , reflecting their unique symmetries of σ_h for D_{5h} and *i* for D_{5d} . For example, staggered D_{5d} gives a symmetric 2D MEP showing the character of the symmetric centre, *i*, whereas the eclipsed D_{5h} provides a butterfly shaped 2D MEP exhibiting a single σ_h plane. Furthermore, the bottom panels, (a₃) and (b₃) are cross-sections through the centre Fe atom parallel to the Cp rings, which clearly indicate that the electron densities at the Fe centre and its vicinity are very different in D_{5h} and D_{5d} conformers. As shown in Fig. 4(a₃), the electron density map of the eclipsed Fc presents a pentagonal MEP, whereas Fig. 4(b₃) reports an electron disk centred at the Fe atom in the staggered Fc. The observation suggests that any properties of ferrocene reflecting such different σ_h and *i* symmetries may be able to differentiate the conformers. This information provides a clue for us to concentrate on the Fe-centred properties in the next sections.

3.3. Infrared (IR) spectroscopy of ferrocene

Fig. 5 compares the simulated infrared spectra of D_{5h} and D_{5d} of ferrocene in the region of $400\text{--}4000 \text{ cm}^{-1}$ using our B3LYP/m6-31G(d) model. The spectrum in red is for D_{5d} but black for D_{5h} . There is not any scaling or manipulation in the present calculations. The IR spectra of ferrocene are relatively simple with only a few transition peaks ($I \neq 0$) caused by vibrations which lead to induced dipole moments due to the absence of permanent dipole moments in ferrocene. The spectra consist of six major peaks, in excellent agreement with the simulated IR spectra ($S = 0$) using the B3LYP/Type-I model from Ref [11]. The IR spectra are very similar in D_{5h} and D_{5d} with only small blue shift in the spectra of the eclipsed (D_{5h}) ferrocene. For example, the clustered IR peaks of the eclipsed D_{5h} conformer in the region $<500 \text{ cm}^{-1}$ (highlighted in a dotted box) show a small blue shift of ca. 12 cm^{-1} . The simulated IR spectra agree well with the major peaks in the experimentally measured IR spectra of ferrocene in vapour [24], except that the entire IR band in the region of $1600\text{--}1750 \text{ cm}^{-1}$ shown in this earlier experiment is missing in theoretical results including the present study and a previous one [11]. It suggests that this medium strong IR band in the experiment [24] might be stemmed by vibrations other than ferrocene, such as impurities and the environment etc.

To further understand the IR spectra of Fc, more detailed analysis is needed. Table 2 reports the IR spectral analysis in the region of $400\text{--}4000 \text{ cm}^{-1}$ for the six major non-zero intensity ($I \neq 0$) transitions in Fig. 5. In this table, the IR frequencies of conformer D_{5h} compare with a recent theoretical study of the same conformer of Fc (D_{5h}) [11] and an earlier experimental study (D_{5d}) of Lippincott and Nelson [24]. The agreement between the present results and recent theoretical results (only for the D_{5h} conformer) [11] is good. However, it is noted that in Ref. [11] the Type-I basis set in the B3LYP/Type-I model uses the 6-31G* basis set for the ligand atoms, such as H and C, but the ECP LanL2DZ basis set for the Fe atom. The calculated IR frequencies of eclipsed ferrocene have been scaled by a number of scaling factors (see Table 1S in the supplementary materials in Ref. [11]). For example, the calculated Fe–C stretching vibrations need a scale factor as large as 1.25 in order to fit the corresponding experimental vibrational frequencies of Lippincott and Nelson [24], whereas one of the scale factors for the C–H stretch vibrations is given as 0.889 [11].

In the present study, the IR frequencies for both D_{5h} and D_{5d} conformers of ferrocene using the B3LYP/m6-31G(d) model are the direct results without any scaling and manipulation. Because the modified m6-31G(d) basis set [26], which incorporates necessary diffuse d-type functions for the first-row transition metals such as Fe, exhibits a more accurate performance than the ECP

LanL2DZ basis set (Type-I) for the iron atom in ferrocene, the m6-31G(d) basis set provides a more appropriate description for the important energy difference between the atomic $3d^1 4s^1$ and $3d^{n-1} 4s^2$ states [26,27]. As a result, the present IR frequencies in the region of $400\text{--}4000\text{ cm}^{-1}$ agree well with experiment without any scaling.

Based on point group theory, there are eight irreducible representations (modes) for each of the D_{5h} and D_{5d} [24] ferrocene conformers. According to the selection rules, five of the modes are IR active modes but three of them are IR inactive. Among the five IR active modes, only two modes will show strong IR transitions, as indicated by their character table. That is,

D_{5h} : $a_1', a_2', e_1', e_2', a_1'', a_2'', e_1'',$ and e_2'' ;
 IR active: $a_1', e_1', e_2', a_2'', e_1''$; where e_1' and a_2'' are strong IR active modes;
 IR inactive: $a_1'', a_2',$ and e_2'' ;

D_{5d} : $a_{1g}, a_{2g}, e_{1g}, e_{2g}, a_{1u}, a_{2u}, e_{1u}, e_{2u}$;
 IR active: $a_{1g}, e_{1g}, e_{2g}, a_{2u}, e_{1u}$; where e_{1u} and a_{2u} are strong IR active modes;
 IR inactive: a_{2g}, a_{1u}, e_{2u} ;

The two modes, i.e., e_{1u} and a_{2u} for D_{5d} and e_1' and a_2'' for D_{5h} produce strong IR spectral lines. As a result, the major IR spectral peaks in Fig. 5 are assigned to e_{1u} and a_{2u} for D_{5d} and e_1' and a_2'' for D_{5h} in Table 2. It is found that the IR frequencies of the D_{5h} and D_{5d} conformers are indeed very similar, the discrepancies are within 5 cm^{-1} for the vibrations in the region above 800 cm^{-1} . For example, the largest frequency mode, a_2' for D_{5h} and a_{2u} for D_{5d} are given by 3268 cm^{-1} and 3267 cm^{-1} , respectively. Larger differences in the IR spectra are shown in the region of $400\text{--}500\text{ cm}^{-1}$. For example, the second smallest mode in this region is given by 488 cm^{-1} for e_1' (D_{5h}) which corresponds to the first (smallest frequency) IR peak at 459 cm^{-1} for e_{1u} (D_{5d}).

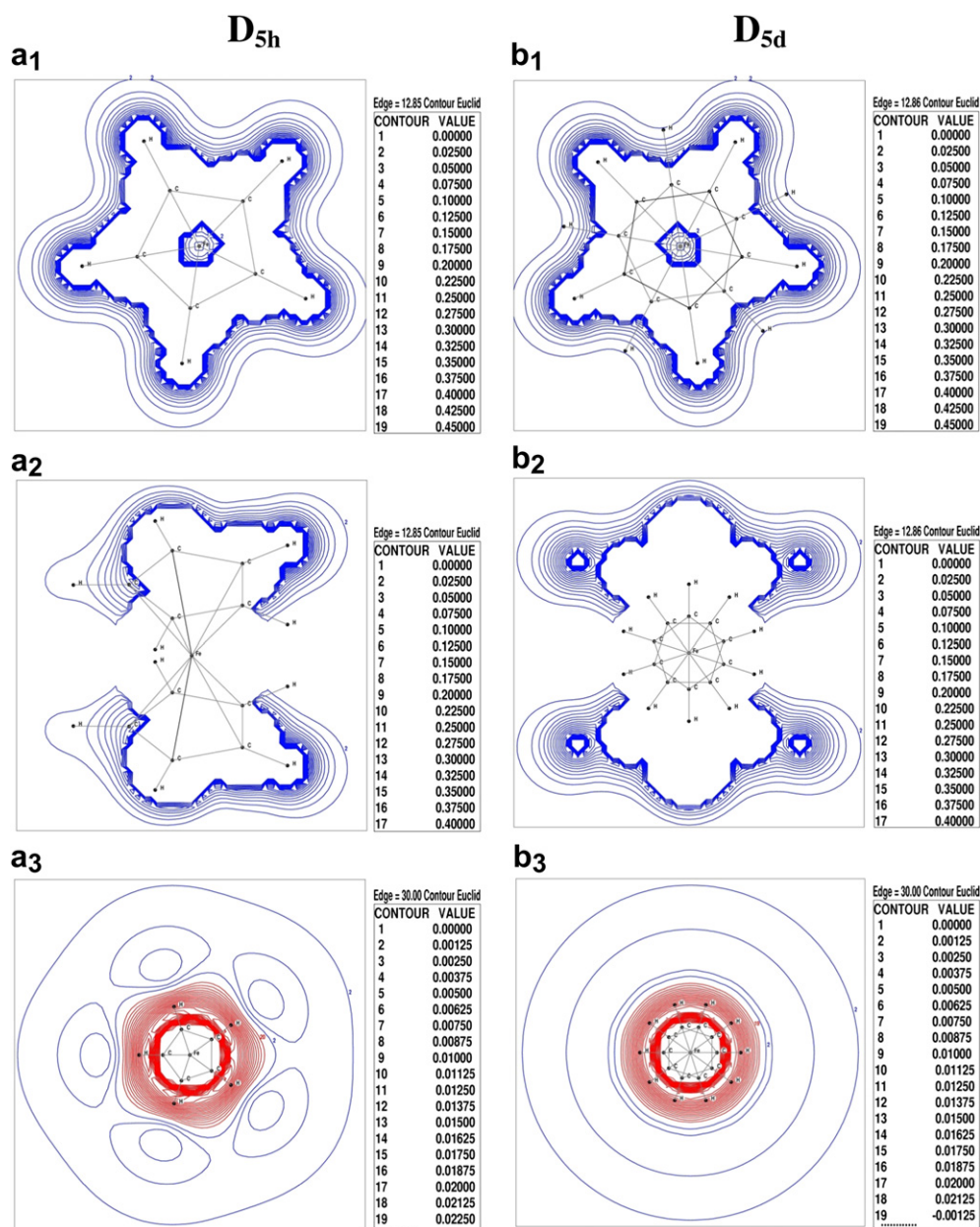


Fig. 4. Two-dimensional cross-sections of the molecular electrostatic potential (MEP) of ferrocene. (a₁) and (b₁), the cross-section through the Cp plane; (a₂) and (b₂) the cross-section through the oblique plane (via Fe) and the Cp ring plane; (a₃) and (b₃) cross-sections through the Fe atom and parallel to the Cp planes.

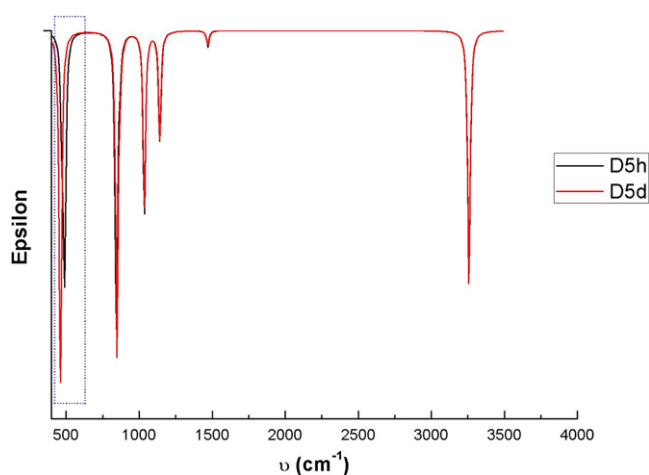


Fig. 5. Comparison of simulated IR spectra of ferrocene, D_{5h} and D_{5d} in vapour phase in the region of $400\text{--}4000\text{ cm}^{-1}$ using the B3LYP/m6-31G(d) model without any scaling. Here the full width at half maximum (FWHM) is 10 cm^{-1} .

3.4. Differentiation of eclipsed and staggered ferrocene conformers

Experimental IR measurement [24] in the $400\text{--}500\text{ cm}^{-1}$ region is indeed reproduced by the present simulation and the IR spectra given by the OPBE/Type-I model (Fig. 2, $S = 0$) in Ref. [11]. In order to reveal more detail Fig. 6 reports the expanded IR spectra of the ferrocene conformers in the region of $400\text{--}650\text{ cm}^{-1}$. The splitting of the first IR spectral peak of the eclipsed ferrocene agrees well with the simulated using the OPBE/Type-I model (Fig. 2, $S = 0$) in Ref. [11]. For example, for the eclipsed Fc, the present calculation gives the IR frequency splitting of $\Delta\nu$ as large as 17 cm^{-1} , which is in excellent agreement with the measured one of 16 cm^{-1} [24].

A closer inspection of the vibration modes of D_{5h} , the mode at 471.23 cm^{-1} (17.75 km mol^{-1}) is a strong vibration being assigned to a_2' , whereas the second spectral line at 488.70 cm^{-1} (22.30 km mol^{-1}) is a stronger vibration with doubly degenerate states being assigned to e_1' , a splitting of $\Delta\nu$ is as large as 17 cm^{-1} between first two IR spectral peaks as shown in Fig. 6 (D_{5h}). Although Gryaznova et al. [11] show only a small splitting of 3 cm^{-1} between 470 cm^{-1} (13 km mol^{-1}) and 473 cm^{-1} (48 km mol^{-1}),

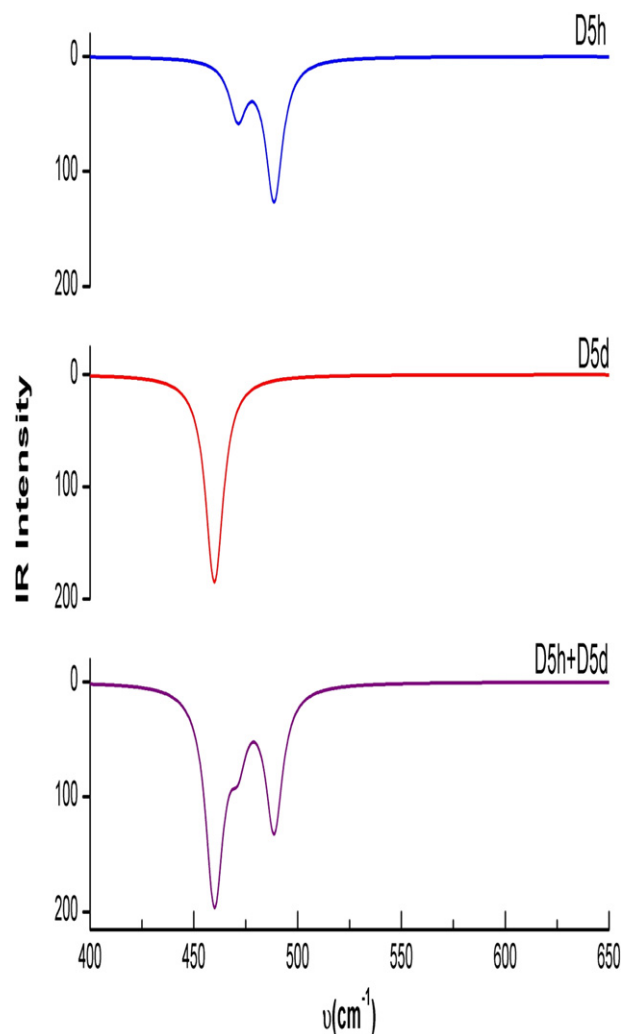


Fig. 6. Comparison of high resolution (FWHM = 5 cm^{-1}) IR spectra of the eclipsed (D_{5h} , blue) and staggered (D_{5d} , red) conformers of ferrocene based on B3LYP/m6-31G(d) model in vacuum in the region of $400\text{--}650\text{ cm}^{-1}$. The synthesized IR spectra of ferrocene by superposition are shown at the bottom panel with purple colour, which indicate the mixture nature of the sample with eclipsed and staggered ferrocene in the measurement. [For interpretation of the references to colour in this figure legend, the reader is referred to the web version of this article.]

Table 2

Calculated IR frequencies and their assignment for the D_{5h} and D_{5d} conformers of ferrocene using the B3LYP/m6-31G(d) model.

D_{5h}		Ref. ^a	D_{5d}		Expt. ^b	Assignment
Mode no.	ν (cm^{-1}) (I (km mol^{-1})), symmetry type	ν (cm^{-1}) (I (km mol^{-1})), symmetry type, Int	Mode no.	ν (cm^{-1}) (I (km mol^{-1})), symmetry type	ν (cm^{-1}), I^c	
7	471 (17.75), a_2''	470 (13), a_2'' , 11	7, 8 ^d	459 (25.54), e_{1u}	480, s	ν FeCp
8, 9	488 (22.30), e_1'	473 (48), e_1' , 16	9 ^e	461 (17.39), a_{2u}	496, s	Ring tilt
18	844(60.31), a_2''	825 (79), a_2'' , 10	18	848 (60.85), a_{2u}	816, s	γ CH
22, 23	870 (1.58), e_1'	841 (10), e_1' , 15	22, 23	871 (1.92), e_{1u}	840, w	Asymmetric γ CH(2 CH upward, 2 CH downward)
30, 31	1035 (17.04), e_1'	1017 (34), e_1' , 14	30, 31	1035 (16.29), e_{1u}	1012, s	δ CCH
37	1141(20.23), a_2''	1141 (15), a_2'' , 9	36	1139 (20.46), a_{2u}	1112, s	Breathing (one Cp shrinks, one Cp expands)
46, 47	1470 (1.55), e_1'	1441 (4), e_1' , 13	44, 45	1469 (1.37), e_{1u}	1416, w	Asymmetric ν CC: Cp, in plane CCH
54, 55	3257 (23.63), e_1'	3123 (46), e_1' , 12	54, 55	3256 (23.88), e_{1u}	3106, m	ν CH
56	3268 (2.75), a_2''	3134 (3), a_2'' , 8	57	3267 (2.54), a_{2u}		ν CH

ν = Stretch; λ = Out of plane; δ = Bend.

^a See [11].

^b See [24].

^c w = weak, m = medium, s = strong.

^d Assignment differs from D_{5h} and is ν FeCp here.

^e Assignment differs from D_{5h} and is ring tilt here.

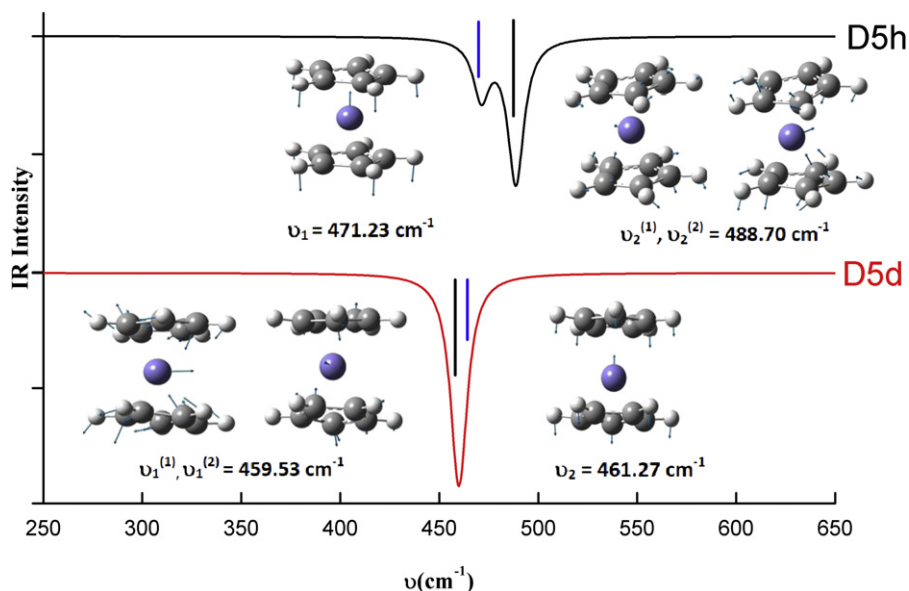


Fig. 7. The IR spectra of the eclipsed (D_{5h}) and staggered (D_{5d}) ferrocene in the fingerprint region produced using the 3D-pdf technique [30]. Double clicking on the structures will activate the embedded 3D structures for related vibrations.

respectively, using the B3LYP/Type-I model, their IR spectra simulated using the OPBE/Type-I model indeed indicate that the higher vibration mode is the stronger vibration being assigned to e_1' , in consistent with simulated spectra in the present study for the eclipsed ferrocene.

Although the IR experiment [24] claimed that the structure of ferrocene was the staggered D_{5d} Fc, the split intensity pattern at ca. 470 cm^{-1} suggests the opposite, i.e., being the eclipsed D_{5h} conformer. If the Fc sample were dominated by the D_{5d} conformer in the experiment, the two spectral lines in the $400\text{--}500\text{ cm}^{-1}$ region should be as close as 2 cm^{-1} (B3LYP/m6-31G*) or 3 cm^{-1} (B3LYP/Type-I) [11]. In addition, the observed first IR spectral peak for D_{5d} in the region of $400\text{--}500\text{ cm}^{-1}$ must be a single and symmetric peak as shown in the middle panel of Fig. 6. If the sample is dominated by the D_{5h} conformer of Fc, however, the first IR spectral peak in the same region is asymmetric and split into two peaks using a spectrometer with higher resolution. The bottom panel is a synthesised IR spectrum of the mixture of D_{5h} and D_{5d} by superposition, the result spectra exhibit an asymmetric peak similar to the IR measurement (Fig. 2 in Ref. [24]), suggesting that the ferrocene sample in the vacuum may be a mixture of the eclipsed and staggered ferrocene conformers.

The vibrations in the IR spectral region near 500 cm^{-1} are dominated by vibrations involving the centre Fe atom. As noted in previous sections (e.g., the MEP), the eclipsed and staggered structures start to show differences when Fe is involved. Fig. 7 gives the vibrations representing the IR peak clusters at ca. $460\text{--}470\text{ cm}^{-1}$ using the recently developed three-dimensional (3D)-pdf animation technique [30] to demonstrate the Fe-centred vibrations. In the eclipsed Fc (D_{5h}), the first IR peak at $\nu_1 = 471.23\text{ cm}^{-1}$ which is assigned to a_2'' is not as strong as the second peak at $\nu_2^{(1)}, \nu_2^{(2)} = 488.70\text{ cm}^{-1}$ which is assigned to the doubly degenerate state of e_1' . The ν_1 peak at 471.23 cm^{-1} of the IR spectrum of eclipsed ferrocene exhibits the vibration in which the Fe atom moves up and down against the flipping directions of the Cp rings. That is, if both the Cp rings flip down, the centre Fe atom moves up and vice versa. The doubly degenerate vibrations of $\nu_2^{(1)}$ and $\nu_2^{(2)}$ of the same conformer (D_{5h}) at 488.70 cm^{-1} engage with the centre Fe atom wobbling left and right, as shown in Fig. 7. The Fe atom plays a central role in these vibrations. Due to the orientation

differences of the Cp rings in the eclipsed ferrocene, the three vibrations present two IR spectral peaks in a 1:2 ratio and a ca. 17 cm^{-1} split. Double clicking on the structures in Fig. 7 will activate the animation of the vibrations.

The vibrations of D_{5d} exhibit a single spectral peak at ca. 460 cm^{-1} . This peak in fact consists of two vibrational lines of one doubly degenerate vibrations of $\nu_1^{(1)}, \nu_1^{(2)} = 459.23\text{ cm}^{-1}$ and a less intensive transition at $\nu_2 = 461.27\text{ cm}^{-1}$. The theory predicts that the transitions are $\Delta\nu = 1.74\text{ cm}^{-1}$ apart which is insufficient to be measured by experiment even with state-of-the-arts high resolution IR technique. The more intensive transition ν_1 of D_{5d} is associated with a doubly degenerate Cp rings flips up and down which leads to the middle Fe atom vibration apparently. The less intensive transition ν_2 at 461.27 cm^{-1} reveals the pentagonal Cp ring wagging vibration which is similar to sugar puckering of tetrahydrofuran (THF) [31–33]. The centre Fe atom of D_{5d} exhibits a left and right wagging vibration (Fig. 7).

4. Conclusions

Infrared (IR) spectra of the eclipsed (D_{5h}) and staggered (D_{5d}) conformers of ferrocene have been simulated using DFT based B3LYP/m6-31G(d) model. It is found that in gas phase, the eclipsed conformer D_{5h} represents the true minimum structure of ferrocene, whereas the staggered conformer D_{5d} represents the saddle point structure, in agreement with a number of other theoretical [9,34] and recent experimental studies [20]. The present study indicates that the sandwich complexes are formed by stacking the two Cp rings with an Fe atom in the middle, rather than being formed with the conventional ten Fe–C bonds as displayed by many of previous studies of ferrocene. It is further discovered in this study that whenever the centre Fe is involved, the eclipsed and staggered structures of ferrocene start to show their unique properties and therefore the conformers can be differentiated through the fingerprints. The 17 cm^{-1} IR frequency splitting in the region of $400\text{--}500\text{ cm}^{-1}$, therefore, becomes one of such fingerprints for the eclipsed conformer of ferrocene. In addition, the present study suggests that the earlier IR spectral measurement of Lippincott and Nelson [24] on ferrocene was indeed a mixture of both eclipsed and staggered ferrocene conformers.

Acknowledgements

NM acknowledges Vice-Chancellors' Postgraduate Research Award at Swinburne University. FW and AG acknowledge the ARC Centre of Excellence for Antimatter–Matter Studies for financial support. FW and CC acknowledge Australian Synchrotron Research Program which is funded by the Commonwealth of Australia under the Major National Research Facilities Program. Finally, thanks are given to the National Computational Infrastructure (NCI) at the Australian National University for an award under the Merit Allocation Scheme and Victorian Partnership for Advanced Computing (VPAC) for supercomputing facilities.

References

- [1] T.J. Kealy, P.L. Pauson, *Nature* 168 (1951) 1039–1040.
- [2] D.E. Bean, P.W. Fowler, M.J. Morris, *J. Organomet. Chem.* 696 (2011) 2093–2100.
- [3] T. Daeneke, T.H. Kwon, A.B. Holmes, N.W. Duffy, U. Bach, L. Spiccia, *Nat. Chem.* 3 (2011) 211–215.
- [4] N.J. Long, *Metallocenes: An Introduction to Sandwich Complexes*, Blackwell Science Inc., 1998.
- [5] Y. Yamaguchi, B.J. Palmer, C. Kutal, T. Wakamatsu, D.B. Yang, *Macromolecules* 31 (1998) 5155–5157.
- [6] M.F.R. Fouda, M.M. Abd-Elzaher, R.A. Abdelsamaia, A.A. Labib, *Appl. Organomet. Chem.* 21 (2007) 613–625.
- [7] D. Osella, M. Ferrali, P. Zanello, F. Laschi, M. Fontani, C. Nervi, G. Cavigliolo, *Inorg. Chim. Acta* 306 (2000) 42–48.
- [8] F.A. Cotton, G. Wilkinson, *Advanced Inorganic Chemistry*, fifth ed. John Wiley & Sons, New York, 1988.
- [9] S. Coriani, A. Haaland, T. Helgaker, P. Jørgensen, *Chem. Phys. Chem.* 7 (2006) 245–249.
- [10] D.R. Roy, S. Duley, P.K. Chattaraj, *Proc. Ind. Natl. Sci. Acad.* 74 (2008) 11.
- [11] T.P. Gryaznova, S.A. Katsyuba, V.A. Milyukov, O.G. Sinyashin, *J. Organomet. Chem.* 695 (2010) 2586–2595.
- [12] E.O. Fischer, W. Pfab, *Z. Naturforsch. B7* (1952) 377–379.
- [13] P.F. Eiland, R. Pepinsky, *J. Am. Chem. Soc.* 74 (1952) 4971.
- [14] J.D. Dunitz, L.E. Orgel, *Nature* 171 (1953) 121–122.
- [15] J.D. Dunitz, L.E. Orgel, A. Rich, *Acta Cryst.* 9 (1956) 373–375.
- [16] R.K. Bohn, A. Haaland, *J. Organomet. Chem.* 5 (1966) 470–476.
- [17] A. Haaland, J.E. Nilsson, *Acta Chem. Scand.* 22 (1968) 2653–2670.
- [18] A. Haaland, J. Lusztzyk, D.P. Novak, J. Brunvoll, K.B. Starowieyski, *J. Chem. Soc. Chem. Commun.* (1974) 54–55.
- [19] P. Seiler, J.D. Dunitz, *Acta Crystallogr. Sect. B* 38 (1982) 1741–1745.
- [20] C.T. Chantler, N.A. Rae, M.T. Islam, S.P. Best, J. Yeo, L.F. Smale, J. Hester, N. Mohammadi, F. Wang, *J. Synchrotron. Radiat.*, [Unpublished results].
- [21] D.C. Cooper, C.J. Yennie, J.B. Morin, S. Delaney, J.W. Suggs, *J. Organomet. Chem.* 696 (2011) 3058–3061.
- [22] U. Schatzschneider, N. Metzler-Nolte, *Angew. Chem. Int. Ed.* 45 (2006) 1504–1507.
- [23] Y. Yamaguchi, W. Ding, C.T. Sanderson, M.L. Borden, M.J. Morgan, C. Kutal, *Coord. Chem. Rev.* 251 (2007) 515–524.
- [24] E.R. Lippincott, R.D. Nelson, *Spectrochim. Acta* 10 (1958) 307–329.
- [25] M.J. Frisch, G.W. Trucks, H.B. Schlegel, G.E. Scuseria, M.A. Robb, J.R. Cheeseman, G. Scalmani, V. Barone, B. Mennucci, G.A. Petersson, H. Nakatsuji, M. Caricato, X. Li, H.P. Hratchian, A.F. Izmaylov, G.Z.J. Bloino, J.L. Sonnenberg, M. Hada, M. Ehara, K. Toyota, R. Fukuda, J. Hasegawa, M. Ishida, T. Nakajima, Y. Honda, O. Kitao, H. Nakai, T. Vreven, J.A. Montgomery, J.E. Peralta Jr., F. Ogliaro, M. Bearpark, J.J. Heyd, E. Brothers, K.N. Kudin, V.N. Staroverov, R. Kobayashi, J. Normand, K. Raghavachari, A. Rendell, J.C. Burant, S.S. Iyengar, M.C.J. Tomasi, N. Rega, J.M. Millam, M. Klene, J.E. Knox, J.B. Cross, V. Bakken, C. Adamo, J. Jaramillo, R. Gomperts, R.E. Stratmann, O. Yazyev, A.J. Austin, R. Cammi, C. Pomelli, J.W. Ochterski, R.L. Martin, K. Morokuma, V.G. Zakrzewski, G.A. Voth, P. Salvador, J.J. Dannenberg, S. Dapprich, A.D. Daniels, Ö. Farkas, J.B. Foresman, J.V. Ortiz, J. Cioslowski, D.J. Fox, Gaussian Inc., Wallingford CT, 2009.
- [26] A.V. Mitin, J. Baker, P. Pulay, *J. Chem. Phys.* 118 (2003) 7775–7783.
- [27] J. Martin, J. Baker, P. Pulay, *J. Comput. Chem.* 30 (2009) 881–883.
- [28] ADF-GUI 2009.01. <http://www.scm.com> (Jan 2012).
- [29] G. Schaftenaar, J.H. Noordik, *J. Comput.-Aided Mol. Des.* 14 (2000) 123–134.
- [30] L. Selvam, V. Vasilyev, F. Wang, *J. Phys. Chem. B* 113 (2009) 11496–11504.
- [31] T. Yang, G. Su, C. Ning, J. Deng, F. Wang, S. Zhang, X. Ren, Y. Huang, *J. Phys. Chem. A* 111 (2007) 4927–4933.
- [32] P. Duffy, J.A. Sordo, F. Wang, *J. Chem. Phys.* 128 (2008) 125102–125110.
- [33] C.G. Ning, Y.R. Huang, S.F. Zhang, J.K. Deng, K. Liu, Z.H. Luo, F. Wang, *J. Phys. Chem. A* 112 (2008) 11078–11087.
- [34] Z.F. Xu, Y. Xie, W.L. Feng, H.F. Schaefer III, *J. Phys. Chem. A* 107 (2003) 2716–2729.
- [35] F. Takusagawa, T.F. Koetzle, *Acta Crystallogr. Sect. B* 35 (1979) 1074–1081.